Multifunctional nanoparticles co-delivering EZH2 siRNA and etoposide for synergistic therapy of orthotopic non-small-cell lung tumor

Zhi-qiang Yuan, Wei-liang Chen, Ben-gang You, Yang Liu, Shu-di Yang, Ji-zhao Li, Wen-jing Zhu, Xiao-feng Zhou, Chun Liu, Xue-nong Zhang

PII: S0168-3659(16)31084-7
DOI: doi:10.1016/j.jconrel.2017.10.025
Reference: COREL 9012

To appear in: *Journal of Controlled Release*

Received date: 26 October 2016
Revised date: 17 May 2017
Accepted date: 14 October 2017

Please cite this article as: Zhi-qiang Yuan, Wei-liang Chen, Ben-gang You, Yang Liu, Shu-di Yang, Ji-zhao Li, Wen-jing Zhu, Xiao-feng Zhou, Chun Liu, Xue-nong Zhang , Multifunctional nanoparticles co-delivering EZH2 siRNA and etoposide for synergistic therapy of orthotopic non-small-cell lung tumor. The address for the corresponding author was captured as affiliation for all authors. Please check if appropriate. Corel(2017), doi:10.1016/j.jconrel.2017.10.025

Multifunctional nanoparticles co-delivering EZH2 siRNA and etoposide for synergistic therapy of orthotopic non-small-cell lung tumor

Zhi-qiang Yuan[a+], *Wei-liang Chen*[a+], *Ben-gang You*[a], *Yang Liu*[a], *Shu-di Yang*[a], *Ji-zhao Li*[a], *Wen-jing Zhu*[a], *Xiao-feng Zhou*[b], *Chun Liu*[c], *Xue-nong Zhang*[a,*]

a Department of Pharmaceutics, College of Pharmaceutical Sciences, Soochow University, Suzhou 215123, People's Republic of China

b. Changshu Hospital of Traditional Chinese Medicine, Changshu 215500, People's Republic of China

c. The hospital of Suzhou People's Hospital affiliated to Nanjing Medical University，Suzhou, 215000，People's Republic of China

+ These two authors contributed equally to the paper.
Correspondence should be addressed to the following:

The Department of Pharmaceutics, College of Pharmaceutical Science, Soochow University, DuShuHu High Education Zone, Su Zhou, Jiang Su Province, People's Republic of China, 215123; Tel/Fax: +86 (0512) 65882087; E-mail: zhangxuenong@163.com

Abstract

Malignant proliferation and metastasis in non-small cell lung carcinoma (NSCLC) are great challenges for effective clinical treatment through conventional chemotherapy. The combinational therapy strategy of RNA interfering (RNAi) technology and chemotherapeutic agents have been reported to be promising for effective cancer therapy. In this study, based on multifunctional nanoparticles (NPs), the simultaneous delivery of etoposide (ETP) and anti-Enhancer of Zeste Homologue 2 (EZH2) siRNA for the effective treatment of orthotopic lung tumor was achieved. The NPs exhibited pH/redox dual sensitivity verified by particle size changes, morphological changes, and *in vitro* release of drugs. Confocal microscopy analysis confirmed that the NPs exhibited endosomal escape property and on-demand intracellular drug release behavior, which can protect siRNA from degradation and facilitate the chemotherapeutic effect respectively. *In vitro* tumor cell motility study demonstrated that EZH2 siRNA loaded in NPs can decrease the migration and invasion capabilities of tumor cells by downregulating the expression of EZH2 mRNA and protein. In particular, an antiproliferation study revealed that the co-delivery of siRNA and ETP in the multifunctional NPs can induce a synergistic therapeutic effect on NSCLC. *In vivo* targeting evaluation showed that cRGDyC-PEG modification on NPs exhibited a low distribution in normal organs and an obvious accumulation in orthotopic lung tumor. Furthermore, targeted NPs co-delivering siRNA and ETP showed superior inhibition on tumor growth and metastasis and produced minimal systemic toxicity. These findings indicated that multifunctional NPs can be utilized as a co-delivery system, and that the combination of EZH2 siRNA and ETP can effectively treat NSCLC.

Keywords

NSCLC, EZH2 siRNA, ETP, NPs, co-delivery system

Scheme 1. (A) Schematic presentation of the formation of co-delivering siRNA and ETP with pH/redox dual-sensitive polymeric materials (cRGDyC-poly (ethylene glycol))$_x$-(chitosan-polymine)$_y$-(lipoic acid)$_z$ (cPCPL/siRNA/ETP NPs). (B) Bioluminescence image of orthotopic lung tumor *in vivo* and *ex vivo*. (C) Schematic of accumulation at the tumor tissue, uptake into tumor cells, endosomal escape, and intracellular trafficking of cPCPL/siRNA/ETP NPs.

Introduction

Non-small cell lung carcinoma (NSCLC) has become a globally serious health problem; its incidence and mortality rates have been rapidly increasing during the past decades[1]. A majority of patients receive unsatisfactory therapeutic effects because of the relapse or metastasis of NSCLC after chemotherapy or resection[2]. In our previous study, paclitaxel loaded micelles have been used to treat orthotopic NSCLC; the treatment exhibited a more effective antiproliferation to tumor compared with Taxol®[3]. Although tumor growth was effectively restrained by chemotherapeutics during the first treatment, a substantial proportion of the mice have suffered from tumor recurrence or metastasis, which resulted in rapid debilitation and then death. Single chemotherapy remained suboptimal in overcoming tumor metastasis, which was induced by intricate mechanisms involving various gene regulations in the cell[4, 5]. Therefore, it is necessary to down-regulate the related genes during the chemotherapy period.

Enhancer of Zeste Homologue 2 (EZH2), a key member of the Polycomb Group (PcG) gene, was overexpressed in a variety of malignancies including breast cancer[6], prostate cancer[7] and NSCLC[8] but scarcely expressed in normal cells of most types. EZH2 regulates pathophysiological processes of tumor by facilitating cell proliferation and cycle progression[9], accelerating cell infiltration[10], and inhibiting cell apoptosis[11]. EZH2 could also inactivate a potent antiangiogenic factor, vasohibin-1, to contribute to tumor angiogenesis, which conduces tumor spread and metastasis[12, 13]. . Fillmore et al. reported that EZH2 targeting could serve as an

appealing strategy for lung cancer therapy, especially for the BRG1- or EGFR-mutant NSCLC, which was resistant to standard chemotherapy[14]. However, Down-regulation of EZH2 gene alone could not completely inhibit the rapid proliferation of tumor, thus increasing the risk of tumor metastasis. Under this circumstance, cancer therapy relying on the combination of gene regulation and chemotherapy was considered to be a potential strategy[15-17].

Etoposide (ETP), a kind of topoisomerase II (topo II) inhibitor, has been proven to be an effective chemotherapy drug for NSCLC[18]. Meanwhile, ETP would be more sensitive to BRG1 or tyrosine kinase inhibitor-resistant mutant NSCLC when the expression of EZH2 was downregulated[14]. RNA interference (RNAi) has been widely applied in the treatment of malignant tumors because of its high efficiency and specificity for target gene silencing[19-21]. Recently, considerable efforts have been devoted to tumor therapy based on the combination of small interfering RNA (siRNA) and chemotherapeutics[22-24]. Two different mechanisms of action could work cooperatively to produce a synergistic or combined effect[25]. Nevertheless, the combination of EZH2 siRNA and ETP for the treatment of orthotopic NSCLC has not been reported.

The co-delivery of siRNA and chemotherapeutic agent have been reported to be significantly effective in tumor treatment than the two-step sequential treatment[16]. To date, various kinds of nanoparticles (NPs) based on polymers have been developed for co-delivery siRNA and drugs. Polyethyleneimine (PEI), a cationic polymer, has been widely used in effectively transfecting a variety of cells *in vitro* because of its buffering capacity which would induce the swelling and rupture of endosomal membrane to generate rapidly release of gene from the endsomes[26-28]. However, the high toxicity, low stability in vivo and poor drug loading capacity of conventional PEI limited its application[29]. Therefore, the modification of conventional PEI to improve its property for carrier have raised great concern[30].. Hu-Lin Jiang et al. reported that the modification of PEI with CS improved its safety without compromising transfection efficiency[29]. Shuai Shi and coworkers have reported that PEI grafted with MPEG-PCL exhibited superior ability in co-delivering genes and

chemical drugs for the treatment of pulmonary metastases[31]. To achieve ideal antitumor effects, the co-delivery systems should not only deliver payloads into the targeting tumor but also precisely release genes and drugs to their respective action sites[32]. Developing smart co-delivery systems that are more adaptable in complex and changeable tumor environment *in vivo* to improve the effect of combination therapy has been in great need..

In this study, we developed a nanoparticle delivery system based on the assembly of pH/redox dual-sensitive polymeric materials (cRGDyC-poly (ethylene glycol))$_x$-(chitosan-polymine)$_y$-(lipoic acid)$_z$ (cRGDyC-PEG-CS-PEI-LA, cPCPL) for the co-delivery of EZH2 siRNA and ETP to orthotopic NSCLC. CS-PEI (CP) with positive charge was as the backbone of the vector and section to load siRNA via electrostatic adsorption. LA was selected as reduction-responsive agents[33] as well as hydrophobic core to load ETP[34]. cRGDyC-PEG modification was expect to prolong circulation time and enhance the targeting ability of the delivery system[35]. The synergistic tumor suppression and tumor metastasis effect of the cPCPL NPs-based co-delivery system for EZH2 siRNA and ETP were evaluated comprehensively via *in vitro* and *in vivo* studies.

Materials

Branched PEI (1.8 kDa) and lipoic acid were purchased from Sigma-Aldrich (St. Louis, MO, USA).Chitosan with molecular weight (MW) of 1000 Da was obtained from Xingcheng Biochemical Co., Ltd. (Nantong, China). cRGDyC was purchased from GL Biochemical Co., Ltd. (Shanghai, China). Methoxy PEG NHS Ester (M-PEG-NHS 3.5 K) and maleimide PEG NHS ester (Mal-PEG-NHS 3.5 K) were purchased from Jenkem Technology Co., Ltd. (Beijing, China). Anti-KMT6/EZH2 antibody was offered by Abcam Co., Ltd. (Shanghai, China). BeyoRT™ cDNA and Horseradish peroxidase-conjugated secondary antibodies were purchased from beyotime Co., Ltd. (Shanghai, China). EZH2 siRNA(sense strand: 5′-GAGGGAAAGUGUAUGAUAATT-3′and anti-sense strand: 5′-UUAUCAUACACUUUCCCUCTT-3′), FAM labeled siRNA(siRNA^{FAM}), negative control siRNA (siNC) and the primers of EZH2 were supplied by GenePharma Co.,

Ltd. (Shanghai, China). Etoposide injection was purchased from Hengrui medicine Co., Ltd. (Jiangsu, China). 1-(3-dimethylaminopropyl)-3-ethyl carbon carbodiimide hydrochloride (EDC·HCl) and N-hydroxysuccinimide (NHS) were purchased from Aladdin-Reagent Co., Ltd. (Shanghai, China). 1,10-dioctadecyl-3,3,30,30-tetramethylindo- tricarbocyanine iodide (DiR) and D-luciferin sodium salt were purchased from Fanbo Biochemicals Co.,Ltd. (Beijin, China). ECMatrix™ was purchased from BD Biosciences Inc. (Heidelberg, Germany). All other reagents were of analytical grade and used without further purification.

Human lung adenocarcinoma cell line luc-A549 was purchased from Heling Biochemicals Co., Ltd. (Hangzhou, China). Female nude mice (age, 4–6 weeks) were provided by the Experimental Animal Centre of Soochow University (Suzhou, China). All animals were kept in an environment that complied with the guidelines for the care and use of laboratory animals by the National Institutes of Health. All animal procedures were performed following the protocols approved by the Institutional Animal Care.

Methods

2.1 Syntheses of PEG-CS-PEI-LA (PCPL) and cPCPL

2.1.1 Syntheses of CP and CS-PEI-LA (CPL)

CP was synthesized using the sodium periodate method[36]. Briefly, CS (0.400 g) and sodium periodate (0.010 g) were dissolved in 30 mL and 10 mL of NaAc–HAc (0.1 M) buffer solution, respectively, at pH 4.5. The sodium periodate solution was added drop-wise to the CS solution under the protection of nitrogen. After stirring for 48 h at 4 °C, the reaction was terminated by 10 mL of ethylene glycol and then dialyzed for 8 h (MW = 3500). PEI (0.360 g) dissolved in 10 mL of water was slowly added to the dialysate and stirred for 48 hours. The reaction was terminated by sodium borohydride (2.000 g), and the resulting solution was continuously dialyzed for 48 h. Following dialysis, the solution was lyophilized to obtain CP.

EDC·HCl (0.384 g) and NHS (0.230 g) were slowly added to LA (0.100 g), dissolved in 10 mL of dimethyl formamide (DMF), and then incubated for 30 min at

room temperature. Subsequently, CS-PEI (0.200 g) dissolved in water was added drop-wise to the above solution. The reaction proceeded for 24 h with gentle agitation at 30 °C. The resulting solution was treated according to the above-described procedure for obtaining CPL.

2.1.2 Grafting of PEG-NHS or cRGDyC-PEG-NHS to CS-PEI-LA

The ploymer was synthesized as described with modification[35]. PEG-NHS (0.050 g) was added to CPL (0.200 g) in 5 mL of borate buffer (0.05 M) at pH 8.0. The reaction solutions were stirred at room temperature for 24 h. The resulting solution was dialyzed for 48 h and then lyophilized to obtain PCPL.

cRGDyC-PEG-NHS was synthesized by the reaction between maleimide group of Mal-PEG-NHS and the thiol group of cRGDyC. cRGDyC (0.020 g) was added to the solution of Mal-PEG-NHS (0.050 g) dissolved in 5 mL of NaAc–HAc buffer (0.1 M) at pH 6.0 and then vortex mixing for 30 s. The generated cRGDyC-PEG-NHS solution was mixed with the CPL (0.200 g) solution dissolved in 5 mL of borate buffer at pH 9.2. The following reaction step was in accordance with the above-described procedure. The final product cPCPL was stored at −20 °C. The intermediate products and final products were characterized by ^{1}H nuclear magnetic resonance (^{1}H NMR) spectroscopy (400 MHz, Varian, Palo Alto, CA, USA).

2.3. Acid–base titration

The buffering capacity of the polymers was measured by the acid–base titration method according to the literature[37]. In brief, 10 mL of NaCl (0.01 M) solution containing 10 mg of CS, PEI,CP, CPL, or cPCPL was adjusted to pH 12.0 using NaOH (1 M) and then titrated with HCl (0.01 M) until the pH value declined to 2. The titration profile was obtained according to the variation of all solution pH values determined with a pH-meter after each titration with 0.2 mL of HCl (0.01 M). The buffer capacity of polymers from pH 7.4 to 5.3 was also calculated according to the following equation:

$$\text{Buffer capacity } (\%) = 100\times (V_{HCL}\times 0.01\ \text{M})/N\ \text{mol}$$

where V_{HCL} is the volume of HCl solution (0.01 M) consumed in the titration of the

polymer solution from pH 7.4 to 5.3 and N mol is the total moles of the protonable amine groups in the polymers.

2.4 Preparation of NPs

cPCPL/ETP (Nile Red or Dir) NPs were prepared by solvent evaporation. In brief, 5 mg of ETP(100 μL Nile Red dissolved in dichloromethane at the concentration of 1 mg/mL) dissolved in dichloromethane was added drop-wise to cPCPL (20 mg) dissolved in 8 mL of water with agitation at 30 °C for 3 h. Then the NPs dispersion was evaporated at 37 °C for 10 min to remove the residual dichloromethane. Free ETP was removed with a 0.22-μm Millipore filter to obtain homogenous NPs dispersion. PCPL/ETP NPs were prepared as described above.

siRNA ($siRNA^{FAM}$) NPS complex was prepared as previously described[38]. siRNA ($siRNA^{FAM}$) solution (1 O.D. siRNA dissolved in 125 mL of DEPC-treated water) was mixed with NPs dispersion using a vortex and then incubated at room temperature for 30 min. The ratio of siRNA ($siRNA^{FAM}$)/NPs complex was optimized by agarose gel-shift assay.

2.5. Characterization of NPs

The drug entrapment efficiency (EE %) and loading capacity (LC %) of cPCPL/ ETP NPs were determined by high-performance liquid chromatography (HPLC) as previously described[39]. The mobile phase comprised methanol–water (70:30, v/v) and the flow rate was 0.7 mL/min at 30 °C. The detection wavelength was 285 nm. The EE % and LC % were calculated using the following equations:

EE %= (weight of encapsulated drug/ weight of total drug) ×100%

LC %= (weight of encapsulated drug/ weight of total drug and vector) ×100%

The particle distribution and zeta potential of cPCPL/siRNA/ETP NPs were measured by dynamic light scattering (Nicomp-380 ZLS particle sizing system, PSS Co., Port Richey, FL, USA) at pH values of 7.4 and 5.3. The sensitive effect of NPs to GSH was also investigated. Each test was repeated three times. The morphology of cPCPL/siRNA/ETP NPs was observed by transmission electron microscopy (TecnaiG220, FEI Company, Hillsboro, OR, USA).

Drug release of ETP/cPCPL NPs was quantified by dialysis. Briefly, 6 mL of cPCPL/siRNA/ETP NPs dispersion (containing 3 mg of ETP) placed in a dialysis bag was submerged into 100 mL of PBS (pH 7.4, pH 7.4+GSH, pH 5.3, and pH 5.3+GSH) with 10% ethyl alcohol under mechanical shaking (100 rpm) at 37 ℃ for 72 h. Aliquots (1 mL) were withdrawn from the outer dialysate and replaced with equal volumes of the medium at predetermined time intervals. The concentration of ETP was measured by HPLC.

2.6 Gel retardation assay

The binding ability of cPCPL to siRNA was accessed by agarose gel electrophoresis. cPCPL/siRNA were formulated in 50 μL of DEPC water at various N/P ratios (0, 1, 2, 4, 8, 16, and 32). Then cPCPL/siRNA NPs dispersion were electrophoresed on a 3% agarose gel containing 5 μg /100 mL Goldview (Amresco, USA) in TAE buffer at 120 V for 25 min. The electrophoretic mobility was revealed *via* UV light irradiation.

Nuclease stability and serum stability of siRNA in the NPs was demonstrated by incubating cPCPL/siRNA NPs with RNase (20 mg/mL) or 10% serum at a predetermined time at 37 ℃. EDTA (0.25 M) was added to inactivate the RNase. Subsequently, siRNA in the NPs were replaced with heparin sodium for incubating for 16 min. The untreated sample was used as the negative control, and the free siRNA was used as the positive control.

2.7 *In vitro* analysis of the co-delivery of chemotherapeutic agent and $siRNA^{FAM}$ into luc-A549 cells.

Flow cytometry (BD FACSCalibur) was used to quantitatively study the cellular uptake of cPCPL/$siRNA^{FAM}$ NPs. Luc-A549 cells were seeded in six-well plates at a density of 2×10^5 cells/well in 2 mL of RMPI-1640 medium for 24 h. The cells were rinsed with PBS and incubated with free $siRNA^{FAM}$, PCPL/$siRNA^{FAM}$, and cPCPL/$siRNA^{FAM}$ for 2 h. Then the cells were washed three times with cold PBS, centrifuged, resuspended, and measured by flow cytometry.

To track the intracellular distribution of co-delivery NPs, confocal fluorescent microscope was used to detect the cPCPL/siRNA^{FAM}/Nile Red double-labeled NPs prepared as described above in cells at different times. In brief, luc-A549 cells (3×10^5) were seeded in glass bottom dish was incubated with cPCPL/siRNA^{FAM} /Nile Red for 0.5, 1, 1.5, and 2 h. After fixation with 3.7% formaldehyde for 10 min, the cell nuclei were stained with Hoechst33258 (5 mg/mL). Then the cells were imaged with LSM 710 confocal microscope and ZEN software (Carl Zeiss, Germany). The endosomal escape of NPs was investigated according to the above procedure. Luc-A549 cells were seeded in a glass bottom dish and incubated with cPCPL/siRNA^{FAM} for 10 min, 0.5, 1, 2, 4, and 6 h. Lysosome was stained with Lyso-Tracker Red and cell nuclei were stained with Hoechst 33258.

2.8 *In vitro* gene silencing effects

2.81 Reverse transcription-PCR (RT-PCR)

Luc-A549 cells were seeded in six-well plates at a density of 3×10^5 cells/well in 2 mL of RMPI-1640 medium for 24 h. Then, the medium was replaced with fresh serum-free medium containing siRNA (100nM)-loaded formulations (Control, free siRNA, cPCPL/ negative control siRNA (siNC), PCPL/siRNA NPs, cPCPL/ siRNA NPs, Lip2000/siRNA). Lip2000/siRNA prepared according to the standard protocol was set as the positive control. cPCPL/siNC was set as the negative control. After incubation at 37 ℃ for 4 h, the transfection medium was replaced with a complete medium and incubated for another 48 h. Total RNA was isolated from the transfected cells by Trizol reagent and then 5 μg of the total RNA was reverse transcribed using first-strand cDNA synthesis kit (Beyotime Institute of Biotechnology) according to the manufacturers' instructions. The obtained cDNA was amplified by PCR according to the previously described protocol. The primers used for PCR amplification were as follows: EZH2 sense strand: 5′-CTAGGGAGTGTTCGGTGACCA-3′ and EZH2 anti-sense strand: 5′-ATTCTGCTGTAGGGGAGACCAAG-3′; GAPDH sense strand: 5′-GGGACCTGACTGACTACCTC-3′ and GAPDH anti-sense strand: 5′-TCATACTCCTGCT- TGCTGAT-3′.

2.82 Western blot (WB) analysis

The transfected cells described in the previous section were incubated with RIPA cell lysis buffer with protease inhibitor for 30 min on ice with gentle shaking. The protein was collected from the supernatant of the lysates by centrifuging for 10 min at 12,000 rpm. The protein concentration was determined using BCA Protein Assay Kit (Beyotime, Shanghai, China). Total protein was separated through 8% SDS-PAGE and then transferred to PVDF membranes. Then, the membranes were incubated with EZH2 monoclonal antibody (1:5000) or anti-β-actin monoclonal antibody (1:1000) overnight at 4 °C. After incubation with goat anti-rabbit IgG-HRP antibody for 2 h, the fluorescence of the blots was detected using Odyssey Infrared Imaging System (LI-COR, NE, USA).

2.9 *In vitro* tumor cell motility study

2.9.1 Migration assay

Luc-A549 transfected cells described in Section 2.8.1 were seeded in six-well plates to achieve a confluence of 80%, and subsequently, a 10-μL pipette tip was used to scratch the cells to get vertical streaks[40]. The medium was replaced with fresh low serum medium (2% fetal bovine serum) after washing twice with PBS. The pictures were observed by fluorescence microscopy (IX51,Olympus) and the scratch width was measured at predetermined times (0, 24, and 48 h).

2.9.2 Invassion assay

The matrigel invassion assay was investigated as previously described[41]. In brief, the transfected luc-A549 cells (1×10^6 cells/mL, 200 μL) were transferred to the top chamber of 24-well transwell plates (8 μm pore size; Corning Star, Cambridge, MA) and 500 μL of complete medium with 10% FBS was added into the bottom chamber. The cells in the top chamber were cultured at 37 °C with 5% CO_2 for 24 h and 48 h, followed by fixing with 4% paraformaldehyde, wiping off unpenetrated cells, and staining with giemsa stain for visualization. The number of cells penetrated through the membrane was counted in five randomly selected fields of view.

2.10 MTT and cell cycle and apoptosis assays

In vitro cytotoxicity of various formulations (Free ETP, PCPL/ETP, cPCPL/ETP, and cPCPL/siRNA/ETP) and polymers (CS, PEI, CP, and cPCPL) on luc-A549 cells were investigated by MTT assay. In brief, luc-A549 cells were seeded into 96-well plates at a density of 5×10^3 cells per well and cultured for 24 h. The medium was placed with fresh medium containing the above formulations or polymers and incubated for 24 h or 48 h. After addition of 20 μL of MTT (5 mg/mL in PBS) to each well for 4 h, 100 mL of DMSO was added to dissolve the formazan crystals. Then, the absorbance was measured at 570 nm with a microplate reader (ELx808, Bio-Tek, USA).

For cell cycle and apoptosis assays, luc-A549 cells were seeded in six-well plates to reach a confluence of 80%. The cells were incubated with formulations including control, cPCPL/siRNA, cPCPL/ETP, and cPCPL/siRNA/ETP (ETP: 30 μg/mL, siRNA: 100 nM) for 24 h or 48 h. Subsequently, the cells were treated according to the instructions of the Annexin V-FITC Apoptosis Detection Kit and Cell Cycle and Apoptosis Analysis Kit (Beyotime). The stained cells were analyzed by flow cytometry.

2.11 Targeted delivery to orthotopic lung tumor

For *in vivo* fluorescence imaging, orthotopic lung tumor was constructed based on luc-A549 as previously described[3]. CPL/DiR, PCPL/DiR, and cPCPL/DiR NPs (80 μg/mL of DiR, 200 μL) were intravenously injected into the mice (n=3) to investigate their biodistribution and tumor-targeting efficacy. At 24 h post-injection, NIR fluorescent images of NPs and the bioluminescence of orthotopic lung tumor were captured using IVIS Spectrum (Caliper Life Sciences). After living imaging, the mice were euthanized and organs were excised for ex vivo imaging.

2.12 *In vivo* antitumor efficacy of the NPs

When the orthotopic lung tumor grew for two weeks, the mice were randomly divided into 6 groups (n=3): (1) PBS, (2) Free ETP, (3) cPCPL/ETP, (4) cPCPL/siNC

(5) cPCPL/siRNA (6) PCPL/siRNA/ETP, and (7) cPCPL/siRNA/ETP (ETP= 15 mg/kg, siRNA= 15.2 nmol/kg). Each dose was administered every other day (total of 5 doses) through injection at the tail vein. The bioluminescence of the tumor was measured every 5 days and the body weight was measured every 2 days after the first administration. After 35 days, the mice were euthanized to harvest organs and tumor mass. Tumor mass was cut into pieces and then incubated with RIPA cell lysis buffer with protease inhibitor for 30 min on ice. The concentrations of EZH2 protein in the tumor tissues were measured by WB as described in Section 2.82.

2.13 Statistical analysis

All data were represented as mean ± standard deviation of three or more samples. Two-tailed student's *t*-test or one-way analyses of variance (ANOVA) was performed in the statistical analysis. Statistical analysis was performed using the SPSS software (SPSS 16; SPSS, Chicago, IL, USA). $P < 0.05$ was considered to be statistically significant ($^{*}P < 0.05$, $^{**}P < 0.01$).

Results and discussion 3.1 Synthesis and characterization of polymers

In this study, we developed a multifunctional co-delivery vehicle, cPCPL, composed of a LA core loading ETP, a PEI layer containing the cargo siRNA and a cRGDyC-PEG modification.Fig. 1B illustrates the ^{1}H NMR spectra of the CS, PEI, CP, CPL, PCPL, and cPCPL polymers. As shown in Fig. 1c, δ 2.52–3.47 ppm (–$NHCH_2CH_2$– of PEI), δ= 3.53–3.77 ppm (H-3, H-4, H-5, H-6, H-60 of D-glucosamine unit), and δ= 4.58 ppm (H-1 of D-glucosamine unit) appeared, which illustrated that CS was successfully grafted to PEI[29, 42]. The proton peaks of LA (–CH2CH2CH2–) appeared at δ=1.35–1.68 ppm in the spectrum of CPL, indicating that LA was grafted to the CP (Fig. 1Bd)[33]. The signals which appeared at δ=3.65–3.75 ppm (–CH2CH2– of PEG) and δ=6.82 and 7.10 ppm (H of benzene ring in cRGDyC) confirmed the synthesis of cPCPL (Fig. 1Bf). The degree of substitution of CS, LA, PEG, and cRGDyC and yield rate of intermediate products are summarized in Table 1 according to the ^{1}H NMR

spectra.

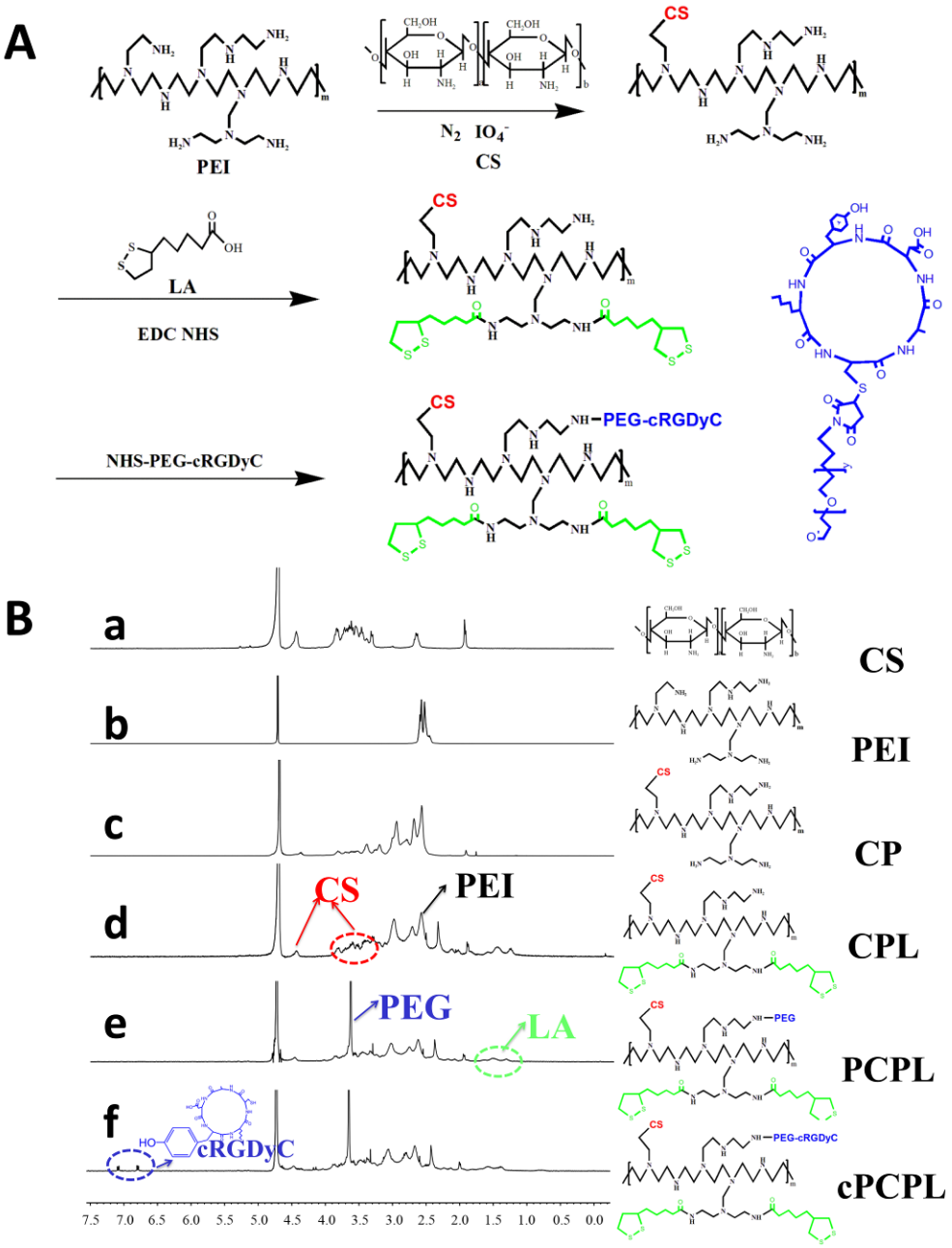

Fig. 1. (A) Synthesis procedures of cPCPL. (B) ^{1}H NMR spectra of (a) CS, (b) PEI, (c) CP, (d) CPL, (e) PCPL, and (f) cPCPL.

3.2 Buffering capacity of the polymers

The buffering capacity of the polymers contributed to the endosomal escape of the NPs into the cytoplasm, thereby reducing the lysosome degradation and improving the

transfection efficiency[43]. As presented in Fig. 2A, PEI consumed more volume of HCl than the other groups from the neutral environment (pH 7.4) to the acidic environment (pH 5.3) in the titration process, which represented theenvironment of blood circulation and endocytic organelles. However, cPCPL exhibited a higher buffer capacity in comparison with PEI (Table.1). This observation may be attributed to the structure of PEI, which had more amine groups than cPCPL at the same concentration. Meanwhile, the buffering capacity of the polymers was mainly determined by the amount of the secondary and tertiary amine groups[44]. The amidation reactions among CS, PEI, LA, and PEG transformed most of the primary amines into secondary amines, increasing the buffer capacity of the cPCPL. Taking advantage of the high buffer capacity, the polymer cPCPL was expected to get a satisfied transfection effect for siRNA.

Table 1 Characterization of polymers.

Ploymer	Degree of Substitution(%)[a]	N(%) [e]	Buffer capacity(%)[f]	Yield rate (%)
CS	--	6.10	8.61	--
PEI	--	27.37	14.12	--
CP	3.17[b]	23.25	10.81	69.7
CPL	15.83[c]	15.10	13.33	91.7
cPCPL	3.21[d]	12.42	17.67	92.3

[a] degree of substitution (DS) defined as number of substituents per 100 nitrogen of PEI calculated by ^{1}H NMR.

[b] DS of CS.

[c] DS of LA.

[d] DS of cRGDyC-PEG.

[e] Determined from elemental analysis.

[f] Measured by acid-base titration.

3.3 Formation and evaluation of cPCPL/siRNA and cPCPL/siRNA/ETP NPs

The binding ability of NPs to siRNA depended on the positive charge of the polymers. PEI, as an integral part of the polymers, endowed positively charged NPs to absorb the negatively charged siRNA. As shown in Fig. 2B (a), the migration of siRNA was completely retarded when cPCPL/siRNA NPs were formed at an N/P ratio of 8. In the prepared cPCPL/siRNA NPs, the N/P ratio between the cPCPL and siRNA was considerably higher than 8, ensuring that siRNA could efficiently bind to the NPs. Nuclease stability assay revealed that NPs could protect the siRNA from nuclease degradation until 120 min (Fig. 2C (c)). However, the brightness band of siRNA was not weakened further at 240 min compared with 120 min. This observation could be attributed to the insertion of siRNA into the depth of NPs, which resulted in better protection. The results of serum stability showed brightness band of siRNA was barely weakened in 240 min which proved NPs could protect the effective transport of siRNA in blood.

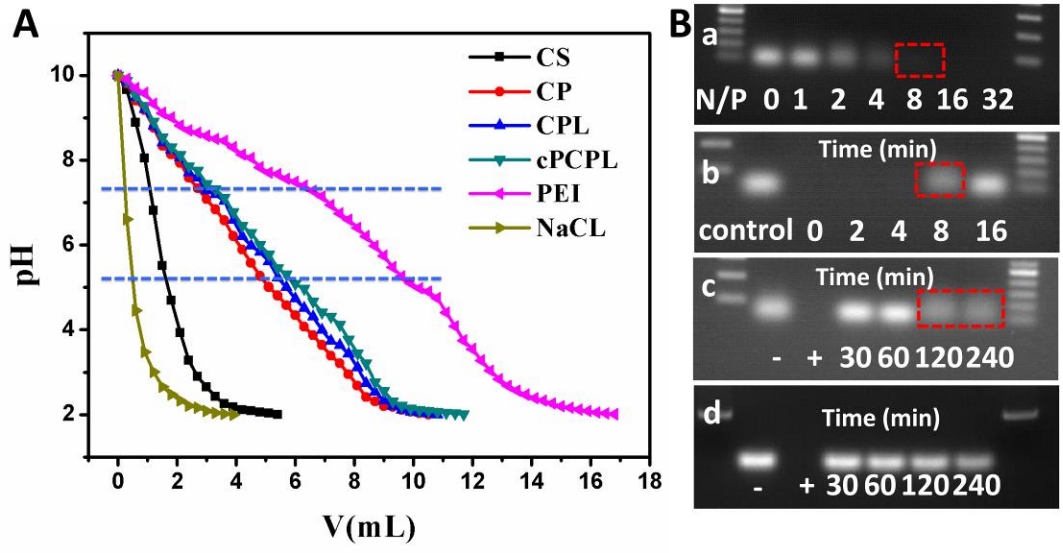

Fig. 2. (A) Acid–base titration profiles of CS, CP, CPL, cPCPL, PEI, and NaCl. (B) Agarose gel retarding assay of cPCPL/siRNA NPs. Binding ability of NPs to siRNA at various N/P ratios (0, 1, 2, 4, 8, 16, and 32) (a). cPCPL/siRNA NPs (siRNA 20 pmol) incubated with heparin to substitute siRNA at 0, 2, 4, 8, and 16 min (b). Nuclease stability (c) or serum stability (d) of siRNA (siRNA 20 pmol) in the NPs was detected by incubating cPCPL/siRNA NPs with Rnase or 10% serum for 30, 60,

120, and 240 min(c) (- negative control; + positive control.).

The co-delivery system was characterized by measuring the particles size and zeta potential at different conditions mimicking blood circulation and tumor microenvironment. The particle size and morphology of cPCPL/siRNA/ETP NPs are shown in Fig. 3A and B. The zeta potential of cPCPL/siRNA/ETP NPs was 7.3±0.4 mV at pH 7.4. The mean particle size of cPCPL/siRNA/ETP NPs was 111.7±3.3 nm (PDI = 0.093;Table. S1) with narrow size distribution and good dispersion at pH 7.4. Under low pH and/or GSH, the mean particle size and size distribution of the NPs became larger and wider, respectively. The amine groups in the polymers protonated at low pH, which makes the surface structure of NPs unstable. Meanwhile, the disulfide bond of LA located in the depth of NPs was reduced to thioalcohol by GSH, thereby destroying the balance of hydrophilic and hydrophobic ends in the polymers. As shown in Fig. 3A, most cPCPL/siRNA/ETP NPs were spherical and uniform at pH 7.4, but were obviously aggregated at pH5.3+GSH. It was assumed that the changes in particles size and morphology would lead to the rapid release of ETP and siRNA under the acidic and reductive conditions.

The release of ETO from co-delivery systems was carried out at different conditions mimicking the blood or tumor environment. *In vitro* release profile of cPCPL/siRNA/ETP NPs was illustrated in Fig. 3C. The ETP released from NPs was less than 40% in 72 h at pH 7.4, which proved that cPCPL/siRNA/ETP NPs could protect ETP from burst release during blood circulation *in vivo*. Low pH or GSH further improved the release rate of drug. In particular, NPs achieved the highest release rate of ETP at pH 5.3+GSH. We predicted that low pH caused the protonation of amino groups in polymers which resulting in structure change of NPs. And disulfide bond was reduced to thiol by GSH which weakened the solubilization capacity of NPs. These two mechanisms coexisted and played roles at the same time, which improved the ETP release rate and amount. Therefore, it was inferred that ETP in NPs would be released rapidly induced by low pH and high concentration GSH in tumor intracellular environment which was beneficial for the chemotherapy of ETP .

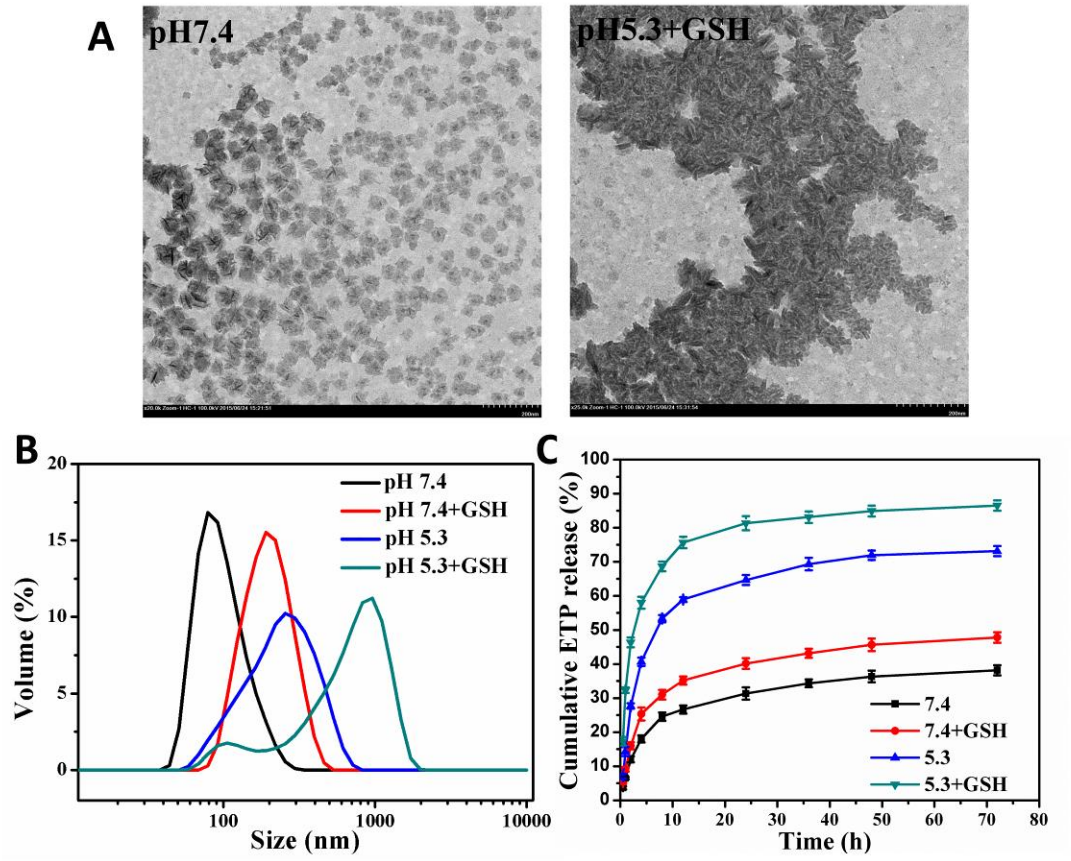

Fig. 3. (A) TEM micrograph of cPCPL/siRNA/ETP NPs at pH 7.4 and pH 5.3+GSH. (B) Size distribution of cPCPL/siRNA/ETP NPs at pH 7.4, pH 7.4+GSH, pH 5.3, and pH 5.3+GSH (treated for 30 min). (C) *In vitro* release of ETP from NPs at pH 7.4, pH 7.4+GSH, pH 5.3, and pH 5.3+GSH. Data represented as mean ± SD (n = 3).

3.4 Cellular uptake, intracellular trafficking, and endosomal escape of NPs

High cellular uptake is the first step to guarantee effective transfection efficiency in the therapeutic application of siRNA. We used flow cytometry to ascertain whether NPs (PCPL/ $siRNA^{FAM}$ and cPCPL/ $siRNA^{FAM}$) could improve the uptake of siRNA to luc-A549 cells. Results showed that NPs considerably improved the cellular uptake of $siRNA^{FAM}$ compared with naked $siRNA^{FAM}$ (Fig. 4A). Moreover, the highest uptake was observed in cRGDyC modified NPs, implying that ligand-mediated effect is conducive to cellular uptake improvement.

Efficient uptake of siRNA is necessary but not sufficient for effective gene silencing effect because endocytosed siRNA needed to escape from endosomes into the cytoplasm[45]. Thus, the endosomal escape of siRNA was evaluated by co-localization of NPs and endo/lysosomes. The endo/lysosomes were stained with Lysotracker Red and NPs labeled by siRNA^{FAM} were visualized as green fluorescence. Fig. 4B revealed green fluorescence (NPs) that was dispersed uniformly in the cytoplasm and co-localized with red fluorescence (endo/lysosomes) gradually within 1 h. At 1.5 h, relatively high co-localization yellow spots of the green and red fluorescence appeared in the cytoplasm. However, a portion of the green fluorescence was dissociated from the red fluorescence at the same time, implying that siRNA started to escape from endo/lysosomes. At 2 h, a high percentage of green fluorescence had significantly dissociated from the red fluorescence (white arrows), indicating the successful escape of siRNA. This occurrence was attributed to the proton sponge effect of cPCPL polymers which absorbed plenty of protons, chloride ions and water into endosomes. We speculated that protons would enhance the surface positive charge of cPCPL polymers and thus form ion pair with negatively charged endosome lipids which resulted siRNA was replaced. The endosome escape of siRNA caused by the proton sponge effect of cPCPL polymers could reduce the lysosome degradation and improve the transfect efficiency of siRNA.

In the co-delivery system, siRNA and ETP produced their effects in the cytoplasm and in the cell nucleus, respectively. Thus, cPCPL/siRNA^{FAM}/Nile Red double-labeled NPs were prepared to explore the specific intracellular distribution of siRNA and ETP. Nile Red was used to represent ETP according to the literature[46]. Fig. 4C exhibited that red fluorescence (Nile Red) and the green fluorescence (siRNA^{FAM}) was co-localization and dispersed uniformly in the cytoplasm at 10 min, 30 min, 1 h, and 2 h. Later, the red fluorescence was obviously dissociated from the green fluorescence (white arrow) and converged to the edge of the cell nucleus, suggesting that siRNA^{FAM} and Nile Red were separated from each other (4h). At 6 h, the red fluorescence overlapped with the blue fluorescence while a high proportion of green fluorescence was still in the cytoplasm. These results implied that cPCPL NPs

could co-deliver siRNA and drugs to their respective target location. These results may be attributed to the reduction sensitivity of the NPs, which are beneficial to drug release in cells.

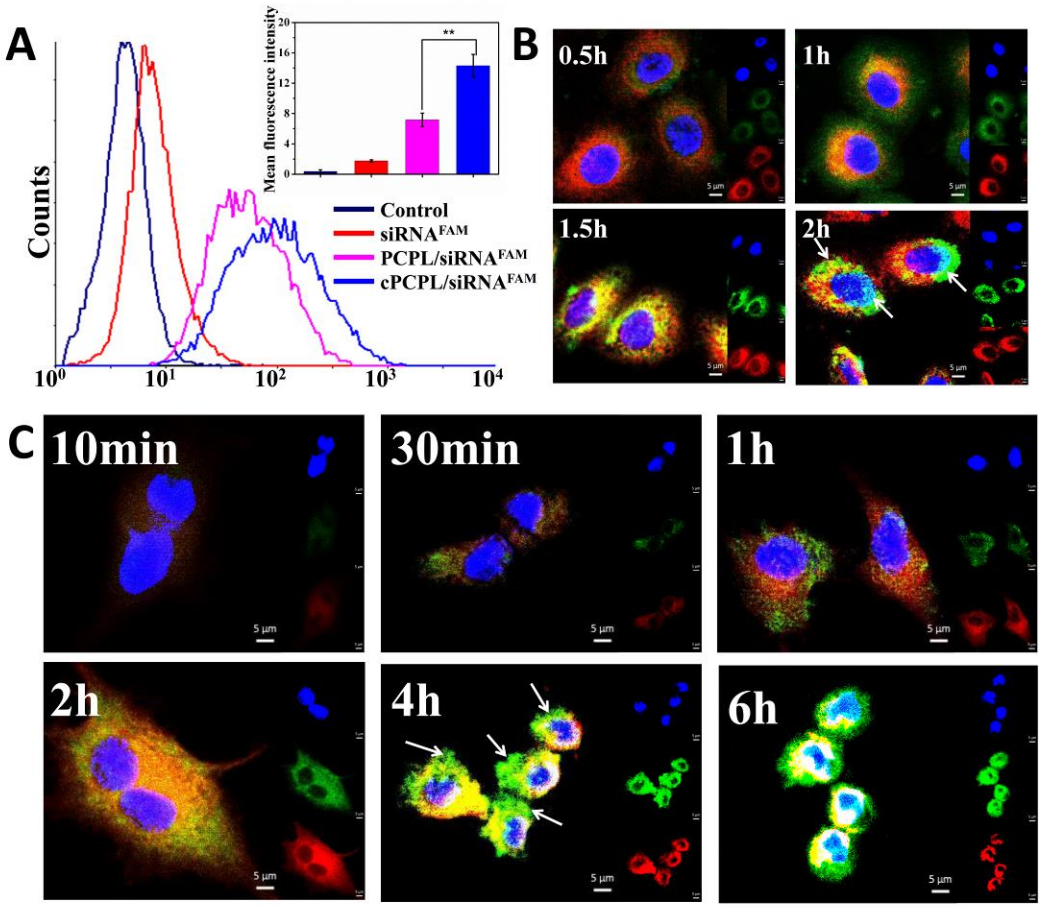

Fig. 4. (A) Cellular uptake of siRNA^{FAM} (100 nM) after 2 h of incubation analyzed by flow cytometry. (B) The endosomal escape of siRNA^{FAM} (100 nM) NPs, and (C) Intracellular trafficking of cPCPL/siRNA^{FAM}/Nile Red (siRNA^{FAM} , 100 nM) double-labeled NPs imaged with an LSM 710 confocal microscope.

3.5 *In vitro* gene silencing of NPs

The EZH2 gene silencing efficiency was evaluated by RT-PCR and Western blot assay. As exhibited in Fig. 5A, the NPs with EZH2 siRNA showed better EZH2 mRNA downregulation effects compared with free siRNA. Moreover, cRGDyC-modified NPs (cPCPL/siRNA) remarkably reduced the expression of mRNA compared with PCPL/siRNA. These results were in agreement with the

cellular uptake described above, indicating that siRNA cPCPL NPs was efficiently delivered into the cytoplasm and that the endosomal escape ability of NPs could greatly improve the efficiency of gene silencing. The protein expression level analyzed using Western blot analysis reconfirmed that efficient gene silencing was induced by cPCPL/siRNA NPs (Fig. 5A (b)). The result of the Western blot analysis was consistent with the RT-PCR assay (Fig. 5B).

3.6 Motility study of tumor cells

Migration assay and invasion assay were used to evaluate whether siRNA NPs could effectively reduce tumor cell motility. As shown in Fig. 4C (a), siRNA NPs could prevent the migration of tumor cells while the scratch area of the control and free siRNA groups were gradually repopulated by cells as time goes on. cPCPL/siRNA NPs were more effective than PCPL/siRNA NPs in inhibiting the tumor cell migrations; this observation was consistent with the results of gene silencing of NPs. Fig. 4C (b) revealed that the least cells penetrated through the matrigel and membrane in cPCPL/siRNA NPs group compared with other groups, suggesting that the NPs decrease the invasion ability of tumor cells. At 48 h, cPCPL/siRNA NPs exhibited significant difference in both scratch width and invasion rate compared with PCPL/siRNA NPs (Fig. 5D) The improvement of cell motility by overexpression of EZH2 provided a basis for tumor metastasis by reduction of cell adhesion and degradation of extracellular matrix[47]. Therefore, cPCPL/siRNA NPs is a potential formulation for inhibiting the metastasis of the tumor by effective downregulation of EZH2 expression.

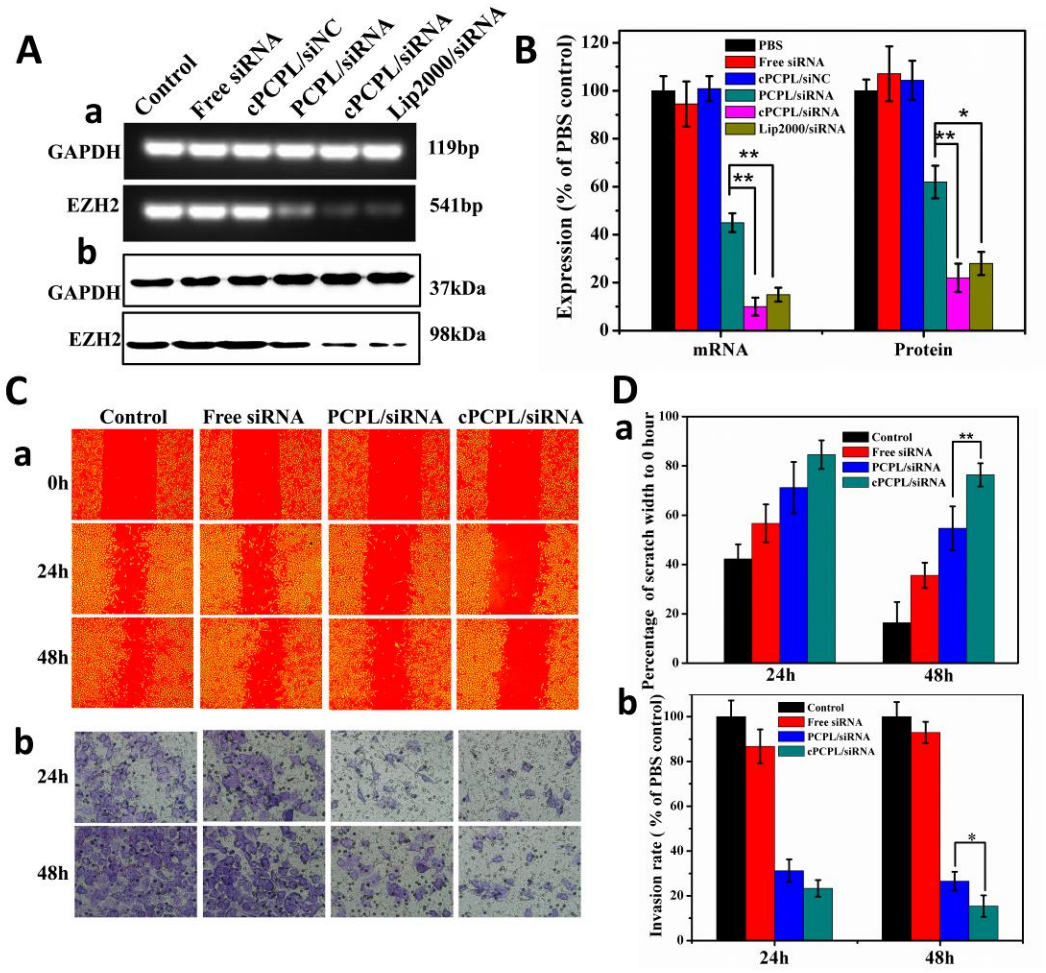

Fig. 5. (A) *In vitro* gene silencing effects detected by RT-PCR (a) and Western blot analysis (b). (B) The relative expression rate of EZH2 mRNA and protein *in vitro*. (C) *In vitro* tumor cell motility study including migration assay (a) and invassion assay (b). (D) Relative cell migration rate (a) and invasion rate (b) at 24 and 48 h. Data represented as mean ± SD (n = 3, *P < 0.05, **P < 0.01).

3.7 *In vitro* antiproliferation study of co-delivery NPs

The cytotoxicity of polymers was determined to evaluate the biocompatibility of the delivery system. Fig. S2 shows that cell viability decreased remarkably with increasing concentrations of CP and PEI-1800, whereas the CS and cPCPL polymer did not exhibit cytotoxicity even at a high concentration (200 μg/mL). The high cytotoxicity of PEI-1800 was mainly caused by destruction of the cell membrane and interference of protein kinase activity[48]. Cell viability was improved after

modification of CS, LA, and cRGDyC-PEG in PEI-1800. This observation may be attributed on one hand, to the decreased proportion of PEI by the introduction of other compounds to the polymers (Table 1), on the other hand, to the reduction of the positive charge of the polymers by PEG to avoid direct stimulation on the cell membrane.

The cytotoxicity of ETP, PCPL/ETP, cPCPL/ETP, and cPCPL/siRNA/ETP was evaluated after incubation with luc-A549 cells for 24 h and 48 h (Fig. 2A and B). As expected, cPCPL/ETP showed higher cytotoxicity to cells compared with ETP and PCPL/ETP because of more cellular uptake. In addition, cPCPL/siRNA/ETP exhibited stronger cytotoxicity to cells with lower IC50 (34.47 μg/mL at 24 h, 15.78 μg/mL at 48 h) than other groups, demonstrating the synergistic antitumor effects of siRNA and ETP. However, no significant difference was observed between cPCPL/ETP and cPCPL/siRNA/ETP at 24 h. However, at 48 h, cPCPL/siRNA/ETP had significantly higher cytotoxicity than cPCPL/ETP ($P < 0.05$). These results indicated that the cytotoxicity of the combined siRNA and ETP was significantly enhanced by prolonging the drug administration time.

To investigate the mechanism of synergism of siRNA and ETP, the cell cycle and apoptosis were investigated in the present work. As shown in Fig. 6C, cPCPL/ETP obviously induced cell apoptosis (31.15% at 24 h; 77.02% at 48 h) while cPCPL/siRNA significantly regulated the cell cycle (S arrest: 19.75% at 24 h; 23.43% at 48 h). Notably, only slight early apoptosis was induced by cPCPL/siRNA, suggesting the cytotoxicity to the cells was mainly attributed to the chemotherapeutic drug ETP rather than to siRNA. cPCPL/siRNA/ETP induced more S arrest and cell apoptosis than cPCPL/ETP or cPCPL/siRNA alone. Meanwhile, similar to the MTT assay described above, obvious difference in cell apoptosis induced by cPCPL/siRNA/ETP was observed between 24 and 48 h (61.65% to 95.99%). The action site of ETP was at topo II, which played a key role in DNA replication period (S phase). S phase was remarkably arrested by siRNA, meaning the time of DNA replication in the cell cycle was extended. The longer the S phase was arrested, the more cytotoxicity of ETP would be generated. Therefore, the simultaneous delivery of

siRNA and ETP by the co-delivery system would obtain a synergistic inhibition effect to the cells *in vitro*, especially at 48 h.

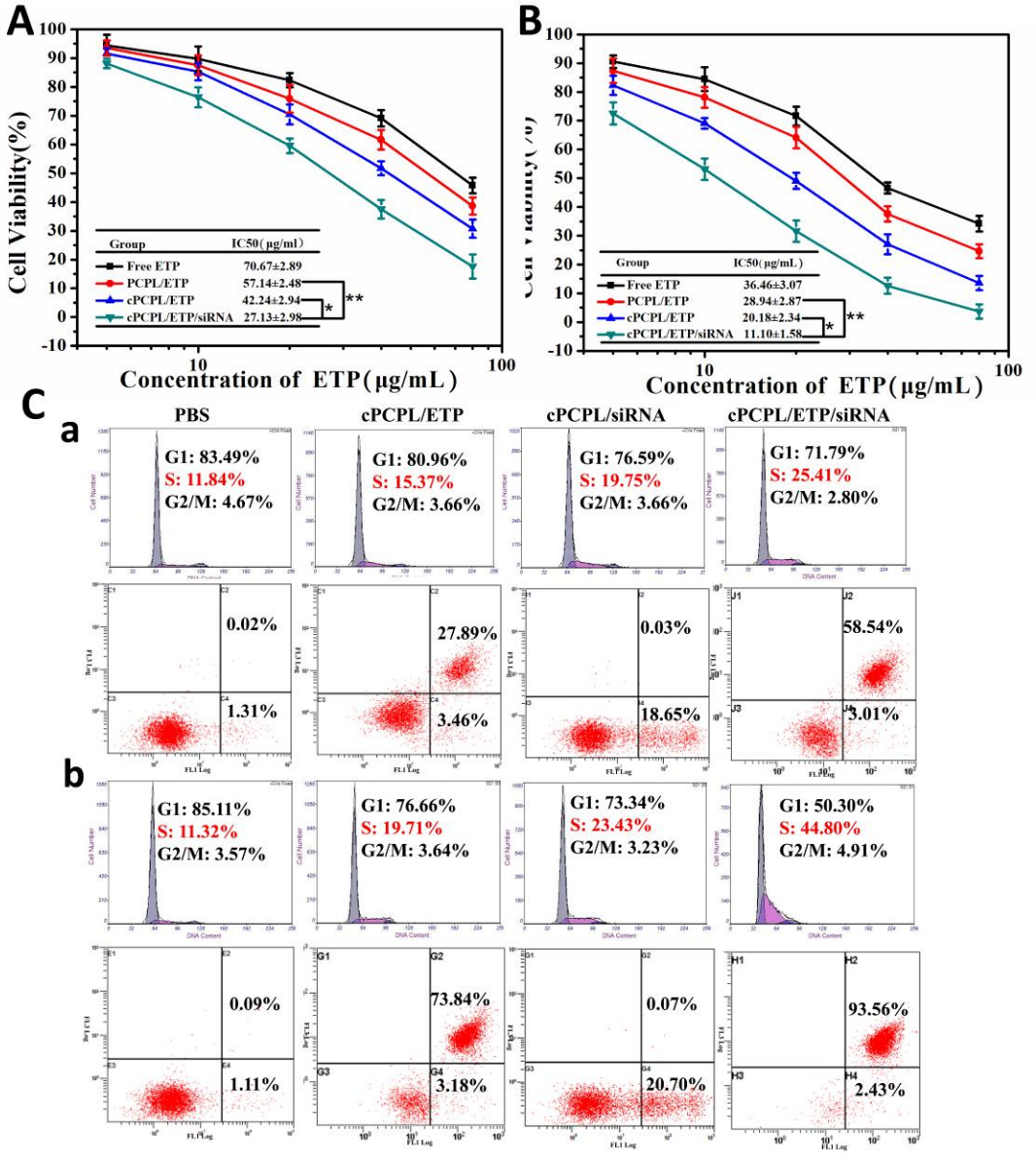

Fig. 6. Cytotoxicity of ETP, PCPL/ETP, cPCPL/ETP, and cPCPL/siRNA/ETP NPs in luc-A549 cells after incubation for (A) 24 h or (B) 48 h. (C) Cell cycle and apoptosis assays of PBS, cPCPL/ETP, cPCPL/siRNA, and cPCPL/siRNA/ETP NPs (ETP: 30 μg/mL, siRNA: 100 nM) at 24 h (a) or 48 h (b). Data represented as mean ± SD (n = 3, *P < 0.05, **P < 0.01).

3.8 Orthotopic lung tumor accumulation and distribution of NPs

In vivo fluorescence imaging system was used to evaluate the distribution of the NPs in nude mice bearing orthotopic lung tumor. The co-delivery systems with relatively small particle size of around 110 nm and cRGDyC-PEG shell was expected to cross the tumor blood vessels easily and accumulate in the tumor site through the EPR and active targeting effect. As shown in Fig. 7A, rainbow bioluminescence was used to determine the location of the tumor mass in the lungs while the red fluorescence (DiR) represented the NPs. Compared with other groups, an obvious accumulation of DiR signal was detected in the lung fields of living imaging in cPCPL/DiR group at 24 h after administration. Without PEG or cRGDyC modifications, the fluorescence signals of NPs were almost held at the liver tissue, suggesting that an obvious nonspecific uptake of NPs by the reticuloendothelial system (RES) occurred. The *ex vivo* images of cPCPL/DiR group showed a more obvious co-localization between the bioluminescence of tumor and the DiR signals in lung compared with PCPL/DiR, implying that cRGDyC was beneficial for NPs to precisely reach the tumor site. Therefore, the cooperation of PEG and cRGDyC modifications would facilitate NPs in accumulating preferentially in the tumor site rather than in normal organs (Fig. 7B).

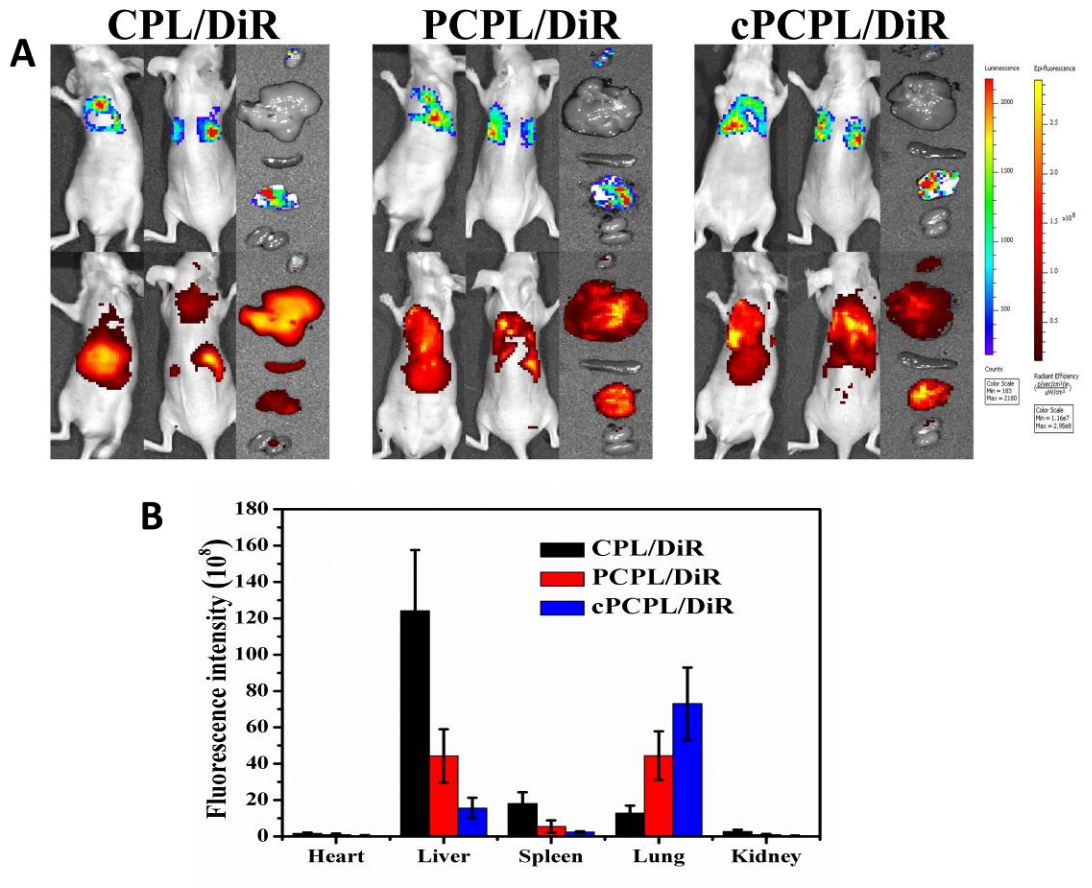

Fig. 7. (A) Orthotopic lung tumor-targeting effects of CPL/DiR (without PEG-cRGDyC), PCPL/DiR (without cRGDyC) and cPCPL/DiR NPs at 24 h. (B) The quantitative data of distribution of DiR labeled NPs in organs.

3.9 Antitumor efficacy of co-delivery NPs *in vivo*

The orthotopic tumor model applied in vivo study presented major differences with the traditional subcutaneous xenograft model. Nude mice bearing orthotopic NSCLC showed a high rate of metastasis, which hardly happened in subcutaneous xenograft model. Moreover, most of the literatures reported that the weight of mice bearing A549 subcutaneous tumor showed an upward trend, which was contrary to the results of mice bearing A549 orthotopic tumor [49-51]. These findings demonstrated that orthotopic tumor model had a higher degree of malignancy compared with subcutaneous xenograft model. The subcutaneous xenograft model may cause the changes of biological characteristics of the tumor cells because of the difference of

microenvironment *in vivo* between visceral organs and subcutaneous tissue[52]. However, the orthotopic tumor model provided same origin of the microenvironment of tumor cells which had a higher clinical relevance[53]. The model, which was more consistent with the tumorigenesis process, may predict anti-tumor efficacy more effectively and reduce the incidence of false positives.

To evaluate the synergistic effect of siRNA and ETP co-delivered by NPs *in vivo*, the bioluminescence intensity of orthotopic lung tumor was set as an index for recording tumor growth. As shown in Fig. 8A, although tumor growth trends were inhibited to some extent after administration of ETP or mono-delivery system, simultaneous delivery of siRNA and ETP appeared to have more potential. After cRGDyC modification, cPCPL/siRNA/ETP NPs suppressed tumor growth more efficiently than PCPL/siRNA/ETP NPs *via* receptor-mediated targeting delivery. The *in vivo* WB results revealed the EZH2 protein expression was significantly downregulated by siRNA *in vivo*, especially for the co-delivery NPs modified with cRGDyC (Fig. 8B). The bioluminescence image of excised organs demonstrated tumor metastasis and accurate distribution (Fig. 8C). The mice treated with PBS or ETP exhibited extensive metastasis foci in livers and kidney. Notably, cPCPL/siRNA moderately inhibited tumor growth in lungs, but fewer tumor mass metastasized to other organs. These results suggested that risk of tumor metastasis was reduced when the expression of EZH2 was downregulated *in vivo*. Moreover, co-delivery systems including siRNA also led to an improved antitumor efficacy of ETP (cPCPL/siRNA/ETP group) via synergistic interaction, corresponding with the results of the *in vitro* antiproliferation study. The body weight of all mice in the treatment groups except ETP increased during the administration, suggesting that the delivery system was safe and even reduced toxicity and ETP side effects (Fig. 8E). No noticeable body weight loss was observed in the cPCPL/siRNA/ETP group, implying that it improved the quality of mice' lives over the course of the study.

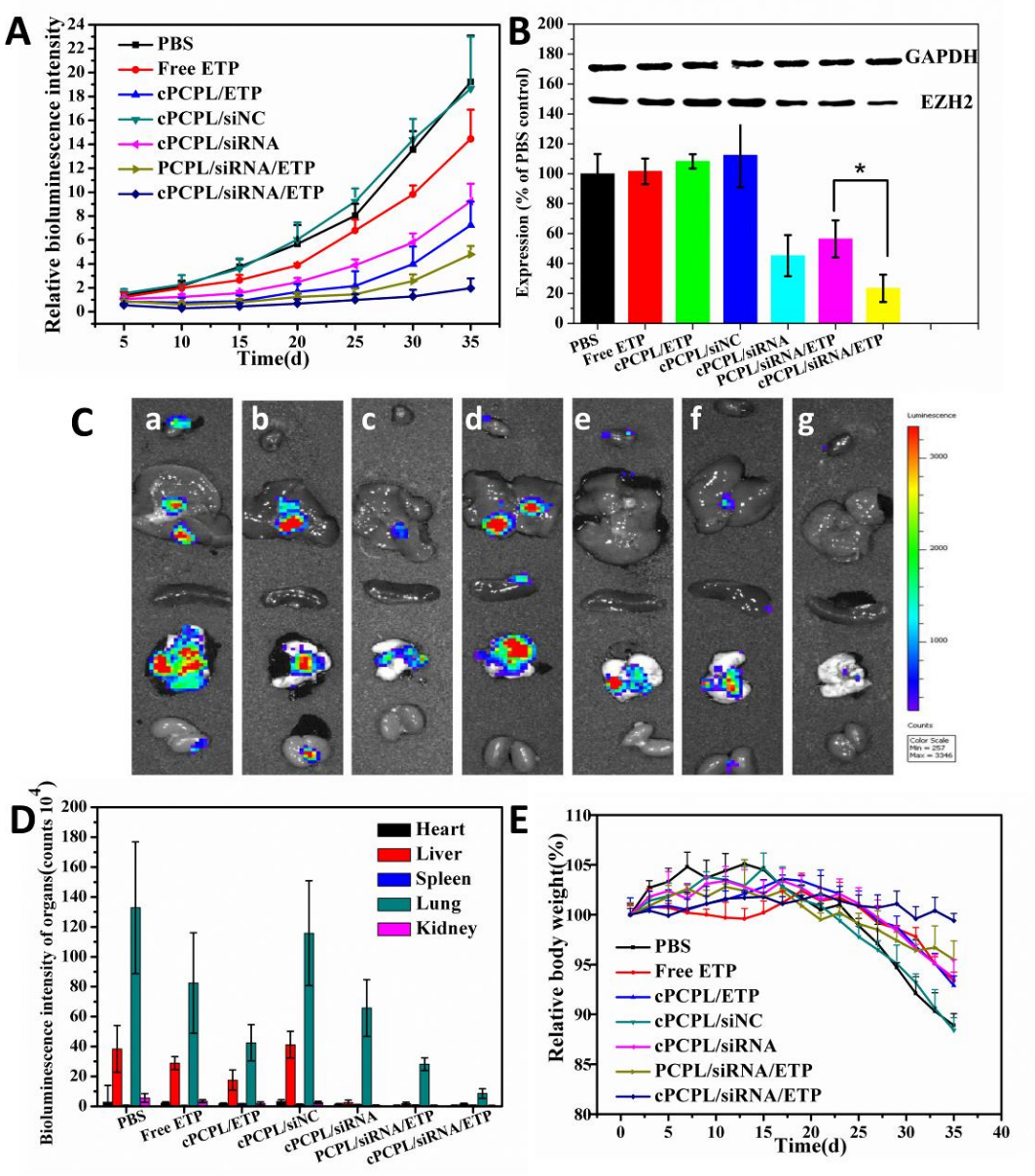

Fig. 8. (A) Variation of bioluminescence of orthotopic tumor under the treatment of various formulations (ETP= 15 mg/kg, siRNA= 15.2 nmol/kg) *in vivo*. (B) Relative expression rate of EZH2 protein in tumor mass. (C) Bioluminescence of tumor mass in the organs (a.PBS, b. Free ETP, c. cPCPL/ETP, d. cPCPL/siNC, e. cPCPL/siRNA, f. PCPL/siRNA/ETP, g. cPCPL/siRNA/ETP. Complete data was shown in Fig. S3.). (D) Bioluminescence intensity of tumor mass of each treatment group in every organ. (E) Relative body weight changes were recorded during the treatment. Relative body weight = body weight/primary body weight. Data represented as mean ± SD (n = 6, *P < 0.05, **P < 0.01).

Conclusion

Overall, we successfully developed a effective and safe delivery system based on multifunctional NPs for the co-delivery of EZH2 siRNA and ETP. The system could synergistically suppress malignant proliferation of orthotopic lung tumor and reduce tumor metastasis. The cPCPL polymers endowed a co-delivery system with pH and redox responsiveness, which resulted in better protection of siRNA and rapid drug release in tumor cells. EZH2 siRNA could not only inhibit cell migration and invasion, but also strengthen the cytotoxicity of ETP via cell cycle regulation. *In vivo* studies revealed that cPCPL/siRNA/ETP NPs significantly inhibited tumor growth and metastasis by targeting delivery and producing low toxicity to the mice. These findings indicated that combined siRNA and ETP therapy using the multifunctional NPs based on cPCPL may be a promising strategy for orthotopic lung tumor treatment.

Acknowledgments

This work was supported by the National Natural Science Foundation projects of China (Nos. 81571788 and 81273463), the Scientific Research Innovation projects of Graduate Students of Jiangsu Universities (CXLX13_840) and the Priority Academic Program Development of Jiangsu Higher Education Institutions (PAPD).

References:

[1]R. Siegel, D. Naishadham, A. Jemal, Cancer statistics, 2012, CA Cancer J Clin 62 (2012) 10-29.

[2]R. Siegel, C. DeSantis, K. Virgo, K. Stein, A. Mariotto, T. Smith, D. Cooper, T. Gansler, C. Lerro, S. Fedewa, C. Lin, C. Leach, R.S. Cannady, H. Cho, S. Scoppa, M. Hachey, R. Kirch, A. Jemal, E. Ward, Cancer treatment and survivorship statistics, 2012, CA Cancer J Clin 62 (2012) 220-41.

[3]Z.Q. Yuan, J.Z. Li, Y. Liu, W.L. Chen, S.D. Yang, C.G. Zhang, W.J. Zhu, X.F. Zhou, C. Liu, X.N. Zhang, Systemic delivery of micelles loading with paclitaxel using N-succinyl-palmitoyl-chitosan decorated with cRGDyK peptide to inhibit non-small-cell lung cancer, Int J Pharm 492 (2015) 141-51.

[4]J. Wen, J. Fu, W. Zhang, M. Guo, Genetic and epigenetic changes in lung carcinoma and their clinical implications, Mod Pathol 24 (2011) 932-43.

[5]C.P. Belani, G. Goss, G.J. Blumenschein, Recent clinical developments and rationale for combining targeted agents in non-small cell lung cancer (NSCLC), Cancer Treat Rev 38 (2012) 173-84.

[6]E.A. Reijm, A.M. Timmermans, M.P. Look, G.M. Meijer-van, C.K. Stobbe, C.H. van Deurzen, J.W. Martens, S. Sleijfer, J.A. Foekens, P.M. Berns, M.P. Jansen, High protein expression of EZH2 is related to unfavorable outcome to tamoxifen in metastatic breast cancer, Ann Oncol 25 (2014) 2185-90.

[7]L. Gu, S.C. Frommel, C.C. Oakes, R. Simon, K. Grupp, C.Y. Gerig, D. Bar, M.D. Robinson, C. Baer, M. Weiss, Z. Gu, M. Schapira, R. Kuner, H. Sultmann, M. Provenzano, M.L. Yaspo, B. Brors, J. Korbel, T. Schlomm, G. Sauter, R. Eils, C. Plass, R. Santoro, BAZ2A (TIP5) is involved in epigenetic alterations in prostate cancer and its overexpression predicts disease recurrence, Nat Genet 47 (2015) 22-30.

[8]J. Kikuchi, I. Kinoshita, Y. Shimizu, E. Kikuchi, J. Konishi, S. Oizumi, K. Kaga, Y. Matsuno, M. Nishimura, H. Dosaka-Akita, Distinctive expression of the polycomb group proteins Bmi1 polycomb ring finger oncogene and enhancer of zeste homolog 2 in nonsmall cell lung cancers and their clinical and clinicopathologic significance,

Cancer 116 (2010) 3015-24.

[9]H. Xia, W. Zhang, Y. Li, N. Guo, C. Yu, EZH2 silencing with RNA interference induces G2/M arrest in human lung cancer cells in vitro, Biomed Res Int 2014 (2014) 348728.

[10]M. Sun, X.H. Liu, K.H. Lu, F.Q. Nie, R. Xia, R. Kong, J.S. Yang, T.P. Xu, Y.W. Liu, Y.F. Zou, B.B. Lu, R. Yin, E.B. Zhang, L. Xu, De W, Z.X. Wang, EZH2-mediated epigenetic suppression of long noncoding RNA SPRY4-IT1 promotes NSCLC cell proliferation and metastasis by affecting the epithelial-mesenchymal transition, Cell Death Dis 5 (2014) e1298.

[11]R. Hubaux, K.L. Thu, B.P. Coe, C. MacAulay, S. Lam, W.L. Lam, EZH2 promotes E2F-driven SCLC tumorigenesis through modulation of apoptosis and cell-cycle regulation, J Thorac Oncol 8 (2013) 1102-6.

[12]T. Hosaka, H. Kimura, T. Heishi, Y. Suzuki, H. Miyashita, H. Ohta, H. Sonoda, T. Moriya, S. Suzuki, T. Kondo, Y. Sato, Vasohibin-1 expression in endothelium of tumor blood vessels regulates angiogenesis, Am J Pathol 175 (2009) 430-9.

[13]K. Watanabe, Y. Hasegawa, H. Yamashita, K. Shimizu, Y. Ding, M. Abe, H. Ohta, K. Imagawa, K. Hojo, H. Maki, H. Sonoda, Y. Sato, Vasohibin as an endothelium-derived negative feedback regulator of angiogenesis, J Clin Invest 114 (2004) 898-907.

[14]C.M. Fillmore, C. Xu, P.T. Desai, J.M. Berry, S.P. Rowbotham, Y.J. Lin, H. Zhang, V.E. Marquez, P.S. Hammerman, K.K. Wong, C.F. Kim, EZH2 inhibition sensitizes BRG1 and EGFR mutant lung tumours to TopoII inhibitors, Nature 520 (2015) 239-42.

[15]A.M. Chen, M. Zhang, D. Wei, D. Stueber, O. Taratula, T. Minko, H. He, Co-delivery of doxorubicin and Bcl-2 siRNA by mesoporous silica nanoparticles enhances the efficacy of chemotherapy in multidrug-resistant cancer cells, Small 5 (2009) 2673-7.

[16]T.M. Sun, Du JZ, Y.D. Yao, C.Q. Mao, S. Dou, S.Y. Huang, P.Z. Zhang, K.W. Leong, E.W. Song, J. Wang, Simultaneous delivery of siRNA and paclitaxel via a "two-in-one" micelleplex promotes synergistic tumor suppression, ACS Nano 5 (2011)

1483-94.

[17]X.B. Xiong, A. Lavasanifar, Traceable multifunctional micellar nanocarriers for cancer-targeted co-delivery of MDR-1 siRNA and doxorubicin, ACS Nano 5 (2011) 5202-13.

[18]R. Zhu, Q. Wang, Y. Zhu, Z. Wang, H. Zhang, B. Wu, X. Wu, S. Wang, pH sensitive nano layered double hydroxides reduce the hematotoxicity and enhance the anticancer efficacy of etoposide on non-small cell lung cancer, Acta Biomater 29 (2016) 320-32.

[19]M.E. Davis, J.E. Zuckerman, C.H. Choi, D. Seligson, A. Tolcher, C.A. Alabi, Y. Yen, J.D. Heidel, A. Ribas, Evidence of RNAi in humans from systemically administered siRNA via targeted nanoparticles, Nature 464 (2010) 1067-70.

[20]C.J. Chen, J.C. Wang, E.Y. Zhao, L.Y. Gao, Q. Feng, X.Y. Liu, Z.X. Zhao, X.F. Ma, W.J. Hou, L.R. Zhang, W.L. Lu, Q. Zhang, Self-assembly cationic nanoparticles based on cholesterol-grafted bioreducible poly(amidoamine) for siRNA delivery, Biomaterials 34 (2013) 5303-16.

[21]A. Reynolds, D. Leake, Q. Boese, S. Scaringe, W.S. Marshall, A. Khvorova, Rational siRNA design for RNA interference, Nat Biotechnol 22 (2004) 326-30.

[22]D. Cheng, N. Cao, J. Chen, X. Yu, X. Shuai, Multifunctional nanocarrier mediated co-delivery of doxorubicin and siRNA for synergistic enhancement of glioma apoptosis in rat, Biomaterials 33 (2012) 1170-9.

[23]T. Yin, L. Wang, L. Yin, J. Zhou, M. Huo, Co-delivery of hydrophobic paclitaxel and hydrophilic AURKA specific siRNA by redox-sensitive micelles for effective treatment of breast cancer, Biomaterials 61 (2015) 10-25.

[24]O. Taratula, A. Kuzmov, M. Shah, O.B. Garbuzenko, T. Minko, Nanostructured lipid carriers as multifunctional nanomedicine platform for pulmonary co-delivery of anticancer drugs and siRNA, J Control Release 171 (2013) 349-57.

[25]F. Greco, M.J. Vicent, Combination therapy: opportunities and challenges for polymer-drug conjugates as anticancer nanomedicines, Adv Drug Deliv Rev 61 (2009) 1203-13.

[26]Y. Xie, N.H. Kim, V. Nadithe, D. Schalk, A. Thakur, A. Kilic, L.G. Lum, D.J.

Bassett, O.M. Merkel, Targeted delivery of siRNA to activated T cells via transferrin-polyethylenimine (Tf-PEI) as a potential therapy of asthma, J Control Release 229 (2016) 120-9.

[27]C. Ganas, A. Weiss, M. Nazarenus, S. Rosler, T. Kissel, G.P. Rivera, W.J. Parak, Biodegradable capsules as non-viral vectors for in vitro delivery of PEI/siRNA polyplexes for efficient gene silencing, J Control Release 196 (2014) 132-8.

[28]E.G. Tierney, G.P. Duffy, A.J. Hibbitts, S.A. Cryan, F.J. O'Brien, The development of non-viral gene-activated matrices for bone regeneration using polyethyleneimine (PEI) and collagen-based scaffolds, J Control Release 158 (2012) 304-11.

[29]H.L. Jiang, J.T. Kwon, E.M. Kim, Y.K. Kim, R. Arote, D. Jere, H.J. Jeong, M.K. Jang, J.W. Nah, C.X. Xu, I.K. Park, M.H. Cho, C.S. Cho, Galactosylated poly(ethylene glycol)-chitosan-graft-polyethylenimine as a gene carrier for hepatocyte-targeting, J Control Release 131 (2008) 150-7.

[30]X. Yue, Y. Qiao, N. Qiao, S. Guo, J. Xing, L. Deng, J. Xu, A. Dong, Amphiphilic methoxy poly(ethylene glycol)-b-poly(epsilon-caprolactone)-b-poly(2-dimethylaminoethyl methacrylate) cationic copolymer nanoparticles as a vector for gene and drug delivery, Biomacromolecules 11 (2010) 2306-12.

[31]S. Shi, K. Shi, L. Tan, Y. Qu, G. Shen, B. Chu, S. Zhang, X. Su, X. Li, Y. Wei, Z. Qian, The use of cationic MPEG-PCL-g-PEI micelles for co-delivery of Msurvivin T34A gene and doxorubicin, Biomaterials 35 (2014) 4536-47.

[32]Z.Z. Yang, J.Q. Li, Z.Z. Wang, D.W. Dong, X.R. Qi, Tumor-targeting dual peptides-modified cationic liposomes for delivery of siRNA and docetaxel to gliomas, Biomaterials 35 (2014) 5226-39.

[33]M. Zheng, Y. Zhong, F. Meng, R. Peng, Z. Zhong, Lipoic acid modified low molecular weight polyethylenimine mediates nontoxic and highly potent in vitro gene transfection, Mol Pharm 8 (2011) 2434-43.

[34]Y. Zhong, J. Zhang, R. Cheng, C. Deng, F. Meng, F. Xie, Z. Zhong, Reversibly crosslinked hyaluronic acid nanoparticles for active targeting and intelligent delivery

of doxorubicin to drug resistant CD44+ human breast tumor xenografts, J Control Release 205 (2015) 144-54.

[35]S. Zhu, L. Qian, M. Hong, L. Zhang, Y. Pei, Y. Jiang, RGD-modified PEG-PAMAM-DOX conjugate: in vitro and in vivo targeting to both tumor neovascular endothelial cells and tumor cells, Adv Mater 23 (2011) H84-9.

[36]I.M. Vold, B.E. Christensen, Periodate oxidation of chitosans with different chemical compositions, Carbohydr Res 340 (2005) 679-84.

[37]M. Wang, H. Hu, Y. Sun, L. Qiu, J. Zhang, G. Guan, X. Zhao, M. Qiao, L. Cheng, L. Cheng, D. Chen, A pH-sensitive gene delivery system based on folic acid-PEG-chitosan - PAMAM-plasmid DNA complexes for cancer cell targeting, Biomaterials 34 (2013) 10120-32.

[38]Q.L. Zhu, Y. Zhou, M. Guan, X.F. Zhou, S.D. Yang, Y. Liu, W.L. Chen, C.G. Zhang, Z.Q. Yuan, C. Liu, A.J. Zhu, X.N. Zhang, Low-density lipoprotein-coupled N-succinyl chitosan nanoparticles co-delivering siRNA and doxorubicin for hepatocyte-targeted therapy, Biomaterials 35 (2014) 5965-76.

[39]Y.C. Kuo, Y.C. Chen, Targeting delivery of etoposide to inhibit the growth of human glioblastoma multiforme using lactoferrin- and folic acid-grafted poly(lactide-co-glycolide) nanoparticles, Int J Pharm 479 (2015) 138-49.

[40]P. Zhang, J. Li, M. Ghazwani, W. Zhao, Y. Huang, X. Zhang, R. Venkataramanan, S. Li, Effective co-delivery of doxorubicin and dasatinib using a PEG-Fmoc nanocarrier for combination cancer chemotherapy, Biomaterials 67 (2015) 104-14.

[41]J. Geng, X. Li, Z. Zhou, C.L. Wu, M. Dai, X. Bai, EZH2 promotes tumor progression via regulating VEGF-A/AKT signaling in non-small cell lung cancer, Cancer Lett 359 (2015) 275-87.

[42]X. Bao, W. Wang, C. Wang, Y. Wang, J. Zhou, Y. Ding, X. Wang, Y. Jin, A chitosan-graft-PEI-candesartan conjugate for targeted co-delivery of drug and gene in anti-angiogenesis cancer therapy, Biomaterials 35 (2014) 8450-66.

[43]H. Hatakeyama, H. Akita, H. Harashima, A multifunctional envelope type nano device (MEND) for gene delivery to tumours based on the EPR effect: a strategy for overcoming the PEG dilemma, Adv Drug Deliv Rev 63 (2011) 152-60.

[44]D.W. Pack, A.S. Hoffman, S. Pun, P.S. Stayton, Design and development of polymers for gene delivery, Nat Rev Drug Discov 4 (2005) 581-93.

[45]B. Lu, C.F. Wang, D.Q. Wu, C. Li, X.Z. Zhang, R.X. Zhuo, Chitosan based oligoamine polymers: synthesis, characterization, and gene delivery, J Control Release 137 (2009) 54-62.

[46]A. Lamprecht, J.P. Benoit, Etoposide nanocarriers suppress glioma cell growth by intracellular drug delivery and simultaneous P-glycoprotein inhibition, J Control Release 112 (2006) 208-13.

[47]C. Lu, H.D. Han, L.S. Mangala, R. Ali-Fehmi, C.S. Newton, L. Ozbun, G.N. Armaiz-Pena, W. Hu, R.L. Stone, A. Munkarah, M.K. Ravoori, M.M. Shahzad, J.W. Lee, E. Mora, R.R. Langley, A.R. Carroll, K. Matsuo, W.A. Spannuth, R. Schmandt, N.B. Jennings, B.W. Goodman, R.B. Jaffe, A.M. Nick, H.S. Kim, E.O. Guven, Y.H. Chen, L.Y. Li, M.C. Hsu, R.L. Coleman, G.A. Calin, E.B. Denkbas, J.Y. Lim, J.S. Lee, V. Kundra, M.J. Birrer, M.C. Hung, G. Lopez-Berestein, A.K. Sood, Regulation of tumor angiogenesis by EZH2, Cancer Cell 18 (2010) 185-97.

[48]K. Kunath, A. von Harpe, D. Fischer, H. Petersen, U. Bickel, K. Voigt, T. Kissel, Low-molecular-weight polyethylenimine as a non-viral vector for DNA delivery: comparison of physicochemical properties, transfection efficiency and in vivo distribution with high-molecular-weight polyethylenimine, J Control Release 89 (2003) 113-25.

[49]J. Shen, Q. Yin, L. Chen, Z. Zhang, Y. Li, Co-delivery of paclitaxel and survivin shRNA by pluronic P85-PEI/TPGS complex nanoparticles to overcome drug resistance in lung cancer, Biomaterials 33 (2012) 8613-24.

[50]M. Li, Z. Tang, S. Lv, W. Song, H. Hong, X. Jing, Y. Zhang, X. Chen, Cisplatin crosslinked pH-sensitive nanoparticles for efficient delivery of doxorubicin, Biomaterials 35 (2014) 3851-64.

[51]W. Zhang, Y. Shi, Y. Chen, S. Yu, J. Hao, J. Luo, X. Sha, X. Fang, Enhanced antitumor efficacy by paclitaxel-loaded pluronic P123/F127 mixed micelles against non-small cell lung cancer based on passive tumor targeting and modulation of drug resistance, Eur J Pharm Biopharm 75 (2010) 341-53.

[52]R.R. Langley, I.J. Fidler, Tumor cell-organ microenvironment interactions in the pathogenesis of cancer metastasis, Endocr Rev 28 (2007) 297-321.

[53]J.J. Killion, R. Radinsky, I.J. Fidler, Orthotopic models are necessary to predict therapy of transplantable tumors in mice, Cancer Metastasis Rev 17 (1998) 279-84.

Scheme 1. (A) Schematic presentation of the formation of co-deliverying siRNA and ETP in pH/redox dual-sensitive polymeric materials (cRGDyC-poly (ethylene glycol))$_x$-(chitosan-polymine)$_y$-(lipoic acid)$_z$ (cPCPL/siRNA/ETP NPs). (B) Bioluminescence image of orthotopic lung tumor *in vivo* and *ex vivo*. (C) Schematic of accumulation at the tumor tissue, uptake into tumor cells, endosomal escape, and intracellular trafficking of cPCPL/siRNA/ETP NPs.

Fig. 1. (A) Synthesis procedures of cPCPL. (B) ^{1}H NMR spectra of (a) CS, (b) PEI, (c) CP, (d) CPL, (e) PCPL, and (f) cPCPL.

Fig. 2. (A) Acid–base titration profiles of CS, CP, CPL, cPCPL, PEI, and NaCl. (B) Agarose gel retarding assay of cPCPL/siRNA NPs. Binding ability of NPs to siRNA at various N/P ratios (0, 1, 2, 4, 8, 16, and 32) (a). cPCPL/siRNA NPs (siRNA 20 pmol) incubated with heparin to substitute siRNA at 0, 2, 4, 8, and 16 min (b). Nuclease stability (c) or serum stability (d) of siRNA (siRNA 20 pmol) in the NPs was detected by incubating cPCPL/siRNA NPs with Rnase or 10% serum for 30, 60, 120, and 240 min(c) (- negative control; + positive control.).

Fig. 3. (A) TEM micrograph of cPCPL/siRNA/ETP NPs at pH 7.4 and pH 5.3+GSH. (B) Size distribution of cPCPL/siRNA/ETP NPs at pH 7.4, pH 7.4+GSH, pH 5.3, and pH 5.3+GSH (treated for 30 min). (C) *In vitro* release of ETP from NPs at pH 7.4, pH 7.4+GSH, pH 5.3, and pH 5.3+GSH. Data represented as mean ± SD (n = 3).

Fig. 4. (A) Cellular uptake of siRNA^{FAM} (100 nM) after 2 h of incubation analyzed by flow cytometry. (B) The endosomal escape of siRNA^{FAM} (100 nM) NPs, and (C) Intracellular trafficking of cPCPL/siRNA^{FAM}/Nile Red (siRNA^{FAM} , 100 nM) double-labeled NPs imaged with an LSM 710 confocal microscope.

Fig. 5. (A) *In vitro* gene silencing effects detected by RT-PCR (a) and Western blot analysis (b). (B) The relative expression rate of EZH2 mRNA and protein *in vitro*. (C) *In vitro* tumor cell motility study including migration assay (a) and invassion assay (b). (D) Relative cell migration rate (a) and invasion rate (b) at 24 and 48 h. Data represented as mean ± SD (n = 3, *P < 0.05, **P < 0.01).

Fig. 6. Cytotoxicity of ETP, PCPL/ETP, cPCPL/ETP, and cPCPL/siRNA/ETP NPs in luc-A549 cells after incubation for (A) 24 h or (B) 48 h. (C) Cell cycle and apoptosis assays of PBS, cPCPL/ETP, cPCPL/siRNA, and cPCPL/siRNA/ETP NPs (ETP: 30 μg/mL, siRNA: 100 nM) at 24 h (a) or 48 h (b). Data represented as mean ± SD (n = 3, *P < 0.05, **P < 0.01).

Fig. 7. (A) Orthotopic lung tumor-targeting effects of CPL/DiR (without PEG-cRGDyC), PCPL/DiR (without cRGDyC) and cPCPL/DiR NPs at 24 h. (B) The quantitative data of distribution of DiR labeled NPs in organs.

Fig. 8. (A) Variation of bioluminescence of orthotopic tumor under the treatment of various formulations (ETP= 15 mg/kg, siRNA= 15.2 nmol/kg) *in vivo*. (B) Relative expression rate of EZH2 protein in tumor mass. (C) Bioluminescence of tumor mass in the organs (a.PBS, b. Free ETP, c. cPCPL/ETP, d. cPCPL/siNC, e. cPCPL/siRNA, f. PCPL/siRNA/ETP, g. cPCPL/siRNA/ETP. Complete data was shown in Fig. S3.). (D) Bioluminescence intensity of tumor mass of each treatment group in every organ. (E) Relative body weight changes were recorded during the treatment. Relative body weight = body weight/primary body weight. Data represented as mean ± SD (n = 6, *P < 0.05, **P < 0.01).

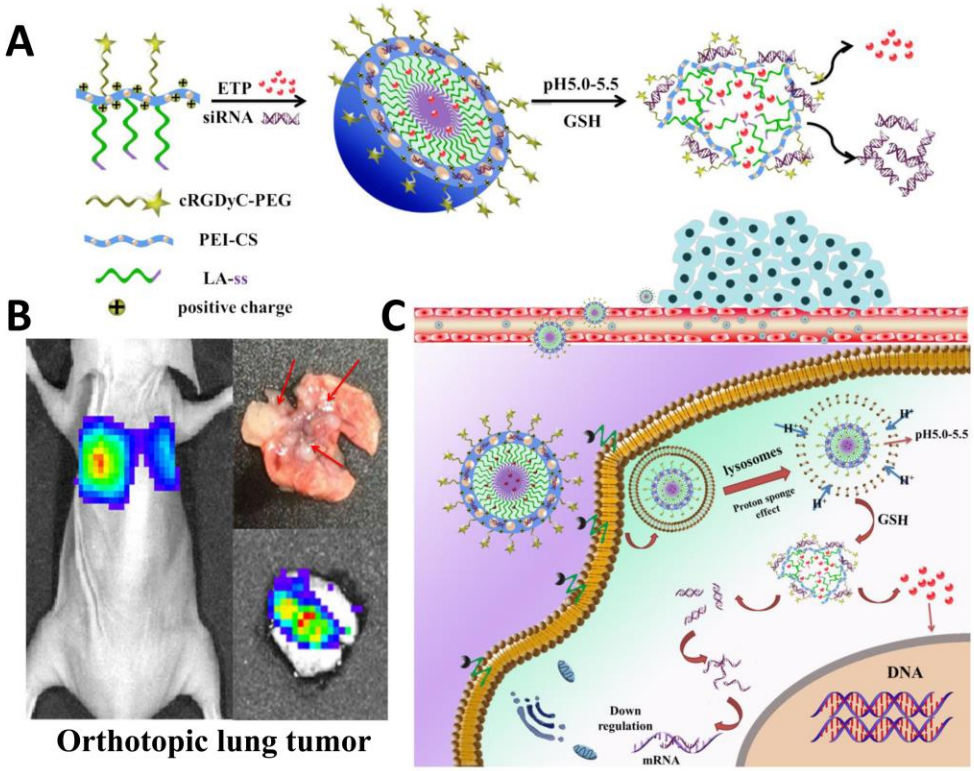

Scheme 1

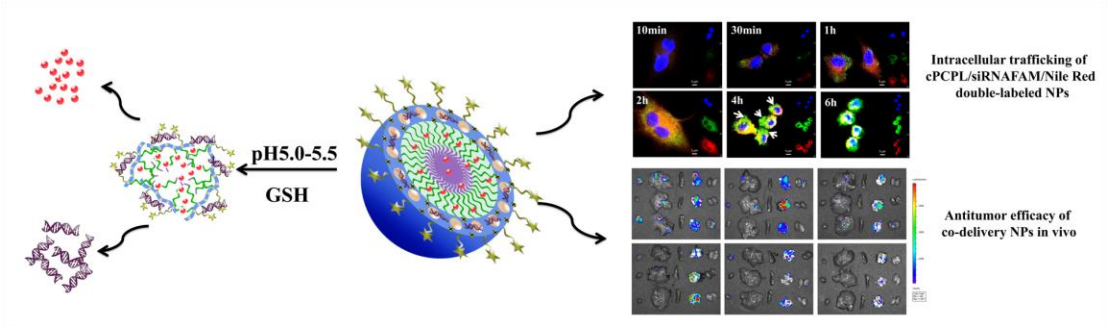

Graphical abstract